USE OF MAGNIFYING MULTIHOLE COLLIMATORS IN THE GAMMA-RAY CAMERA SYSTEM

S. Rudin, P. A. Bardfeld, and H. Hart

Montefiore Hospital and Medical Center, Bronx, New York

There has been much recent interest in the improvement of spatial resolution for radioisotopic scanning systems (*1–6*). The resolution of the Anger camera for line sources (*7,8*) and space sources (*8*) has been discussed and measured using straight-bore, multihole collimators (*9*) and more recently, using a diverging high-energy collimator (*10*). One of the basic restrictions on camera resolution is the inability of the standard system of 19 discrete photomultiplier tubes to effectively localize scintillations within less than a distance r_{PM}, of about 1 cm (Fig. 1, Ref. 8). If the image of the scanned organ can be magnified at the crystal stage, then the subsequent intrinsic fixed blurring of the photomultiplier system is relatively less significant in limiting the resolution obtainable. Such magnification, although decreasing the effective field of view of a camera with a given crystal area (which might not otherwise be in effective use anyway) may make it possible for the photomultiplier-tube system to resolve objects previously unresolvable.

In the next section of this paper a theoretical treatment of the effect of image magnification upon the system modulation transfer characteristics is presented. In the following section experimental results on phantoms using a magnifying multihole collimator are displayed.

EFFECT OF CRYSTAL IMAGE MAGNIFICATION ON INTRINSIC CAMERA RESOLUTION

Assume that the instrumentation following the crystal stage, that is, the photomultiplier tubes and associated circuitry, has a blurring effect roughly described by a normalized Gaussian curve with characteristic spread r_{PM} around the crystal image reference point x_0. The normalized Gaussian curve $g(x)$ is then given by

$$g(x) = \frac{1}{\sqrt{\pi}\, r_{PM}} e^{-(x-x_0)^2/r_{PM}^2}. \qquad (1)$$

Received May 13, 1970; revision accepted July 9, 1971.

For reprints contact: Stephen Rudin, Section of Nuclear Medicine, Montefiore Hospital and Medical Center, 111 E. 210th St., Bronx, N.Y. 10467.

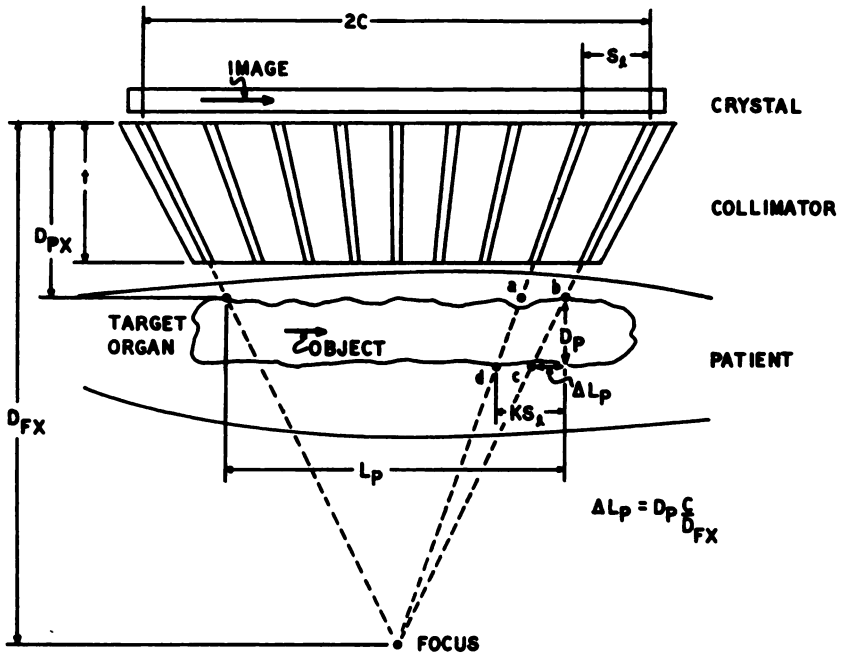

FIG. 1. Magnifying collimator geometry and parameters.

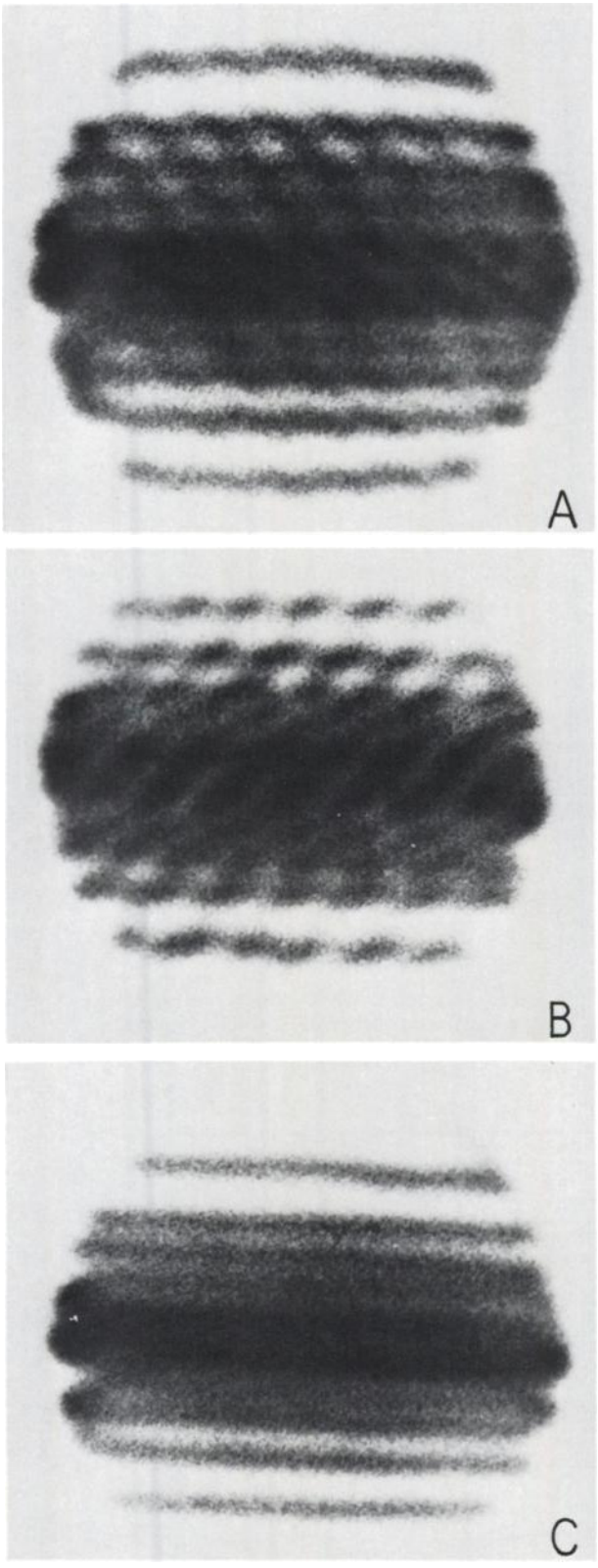

FIG. 2. A shows image of 12-line phantom with ^{99m}Tc using magnifying 1,000-hole collimator (MB1K). B and C show image using standard straight-bore 1,000-hole (SB1K) and straight-bore 4,000-hole (SB4K) collimators, respectively. In all pictures, same number of counts were collected and same dot intensity settings were used. See text for discussion of results with collimators shown in A, B, C, and D.

Two ideal points or line sources ideally collimated to point or line images on the crystal are said to be resolved if their images on the output oscilloscope are separated by a distance greater than their full widths at half maximum (FWHM). By forming magnified crystal images of the point or line sources, the actual resolvable source separations are reduced by the factor 1/M, where M is the magnification.

The effect of magnifying the image at the crystal on the complete system modulation transfer function can be readily determined. Let the image on the crystal be $(1 + \cos \omega x)$, where x is the distance along the crystal and ω is the spatial frequency. Then the resulting blurred image is given by:

$$I(x_0) = \frac{1}{\sqrt{\pi}\, r_{PM}} \int_{-\infty}^{\infty} e^{-(x-x_0)^2/r_{PM}^2} [1 + \cos \omega x]\, dx \quad (2a)$$

$$= 1 + e^{-\omega^2 r_{PM}^2/4} \cos \omega x_0. \quad (2b)$$

It follows that:

$$MTF = \frac{I_{max} - I_{min}}{I_{max} + I_{min}} = e^{-\omega^2 r_{PM}^2/4} \quad (3)$$

in agreement with previous calculations (*11*). If the image at the crystal is magnified by a factor M, the spatial frequency becomes ω/M, with a new MTF of $e^{-\omega^2 r_{PM}^2/4M^2}$. Thus the ratio of modulation transfer function with and without magnification is

$$\frac{MTF\ (\omega/M)}{MTF\ (\omega)} = e^{-\omega^2 r_{PM}^2/4(M^2 - 1/M^2)}. \quad (4)$$

For $\frac{\omega^2 r_{PM}^2}{4} > 1$, a significant improvement in the MTF can result.

The improvement in MTF indicated in Eq. 4 is unaffected by purely collimator-induced blurring because there should be little change in this blurring between a magnifying multihole collimator of moderate taper and a corresponding straight-bore collimator if the number of channels and the thickness are unaltered.

The above analysis has, of course, been restricted to plane parallel sources. For actual three-dimensional organ isotope distributions, lateral positioning ambiguities arise from the oblique channel angulation. A detailed discussion of optimal design parameters for magnifying focusing collimators and alternate pinhole configurations will be presented elsewhere.

RESULTS AND DISCUSSION

In this study three collimators, all made by Nuclear-Chicago Corp., were used. The standard 4,000-hole and 1,000-hole straight-bore collimators, which

we call SB4K and SB1K, respectively, were compared with the 1,000-hole diverging collimator turned over so that it became a magnifying collimator, called MB1K (see Fig. 1). It was not possible to study the performance of a corresponding 4,000-hole diverging collimator since they are not currently available.

A line phantom similar to that of Jahns and Hine (7) was employed consisting of thin plastic tubing forming a 12-line pattern symmetrical around the center and with spacings from the end 2.5, 1.75, 1.25, 1.25, .75, 1.00, .75, 1.25, 1.25, 1.75, 2.5 cm. Figure 2 shows the images of the line phantom containing ^{99m}Tc for the three collimators SB4K, SB1K, and MB1K. The diagonal stripes for the 1,000-hole collimators are due to the hexagonal hole patterns of the collimators which were not aligned with the line phantom. Since the image of the line phantom is clearly visible, this diagonal artifactual pattern can be neglected in comparing line resolution for these two collimators. The SB4K has a square-hole array with smaller holes so that an interfering pattern does not appear. A corresponding 4,000-hole magnifying collimator would not show the artifactual pattern on magnified images. For MB1K (Fig. 2A), the 12-line phantom gives rise to a 10-line image since the two sets of 0.75-cm spaced lines merge into two just resolvable intense bands. The 1-cm spacing between the two sets of lines and the 1.25-cm spaced lines just outside these bands are well resolved. The 1,000-hole straight-bore collimator (SB1K) does not evidence the 1-cm central gap (only a single broad band appears), and 1.25-cm spacings are but marginally represented (Fig. 2B). In Fig. 2C, the result using SB4K (the 4,000-hole straight-bore collimator) appears. Note that while the central "bands" are resolved, the 1.25-cm separated lines are only vaguely represented.

Figure 3 shows the result using ^{131}I in the phantom. In Figs. 3A and B the MB1K and SB1K images appear. The SB1K image has been photographically enlarged 1.2 times to facilitate the comparison. The counting rate/mCi for MB1K ranged from about 1.0 to 0.7 that of SB1K depending upon the position of a given point source in the field of view. A somewhat longer time therefore was required in general to obtain equivalent statistics for the magnifying system. However, the improved resolution herein reported was still demonstrable in pictures obtained with $\sim 1/7$ the counts and $\sim 1/5$ the time, as can be seen from Fig. 3C.

Since obliquity considerations play a role in limiting the usefulness of magnifying collimation, a three-dimensional volume phantom was scanned as well. Figure 4 shows the rectangular volume phantom

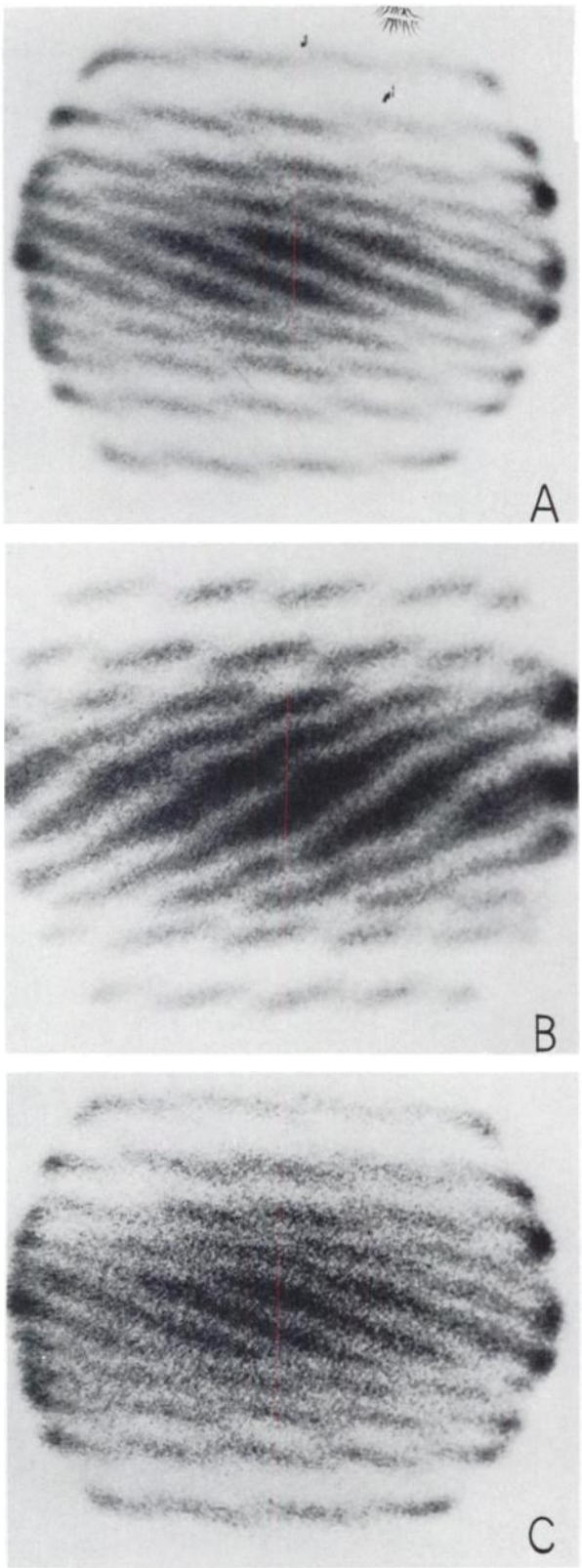

FIG. 3. A shows image of 12-line phantom with ^{131}I using magnifying 1,000-hole collimator (MB1K). B shows image using straight-bore 1,000-hole collimator (SB1K) but photographically enlarged 1.2 times. Number of counts collected in A and B were same as that in Fig. 1. In C, MB1K was used; however, only 1/7 number of counts as in A was collected and dot intensity was increased to give approximately same film density as in A and B.

designed by Treves and Spencer (*12*). Figure 5 shows the image of the volume phantom using ^{99m}Tc for the three collimators. Again the image using the magnifying collimator was better resolved, as can be seen especially by following the left-of-center band vertically downward in the picture.

CONCLUSIONS

It is shown theoretically that the modulation transfer function can be improved by appropriate magnification of the crystal image.

A diverging Nuclear-Chicago collimator, inverted to magnify the gamma-ray image at the crystal, was used to scan line and volume phantoms. These pictures appear to be somewhat better resolved than those employing straight-bore collimators.

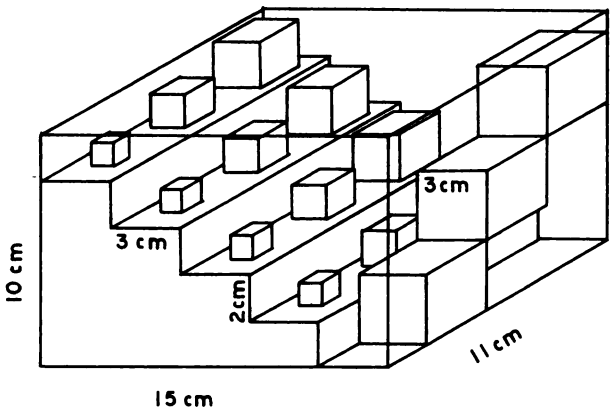

FIG. 4. Schematic diagram of Treves-Spencer volume phantom. First part is composed of three steps, each of which has on it three solid cubes with sides 1, 1.5, and 2 cm. Second part contains three solid cubes with 3-cm side placed at different depths. Isotope in solution is allowed to remain above steps and cubes as well as below two raised 3-cm cubes.

ACKNOWLEDGMENT

We would like to thank Mrs. Kay Pacher for her patience in working with the manuscript, and S. Treves and R. Spencer for permission to use their volume phantom.

REFERENCES

1. ROLLO FD, SCHULZ AG: A contrast efficiency function for quantitatively measuring the spatial-resolution characteristics of scanning systems. *J Nucl Med* 11: 53–60, 1970

2. HART HE, WARSHAW B, STOLLER HI: Geometric efficiency and other performance characteristics of focusing collimators. *IEEE Trans on Biomedical Engineering,* vol BME-14 No 2, 1967, pp 96–102

3. WESTERMAN B, SHARMA RR, FOWLER JF: Relative importance of resolution and sensitivity in tumor detection. *J Nucl Med* 9: 638–640, 1968

4. WILCOX FW, EDGAR WH, BROWN WR: Collimator selection for scintillation camera brain scanning. *J Nucl Med* 10: 297, 1969

5. KELLER EL: Optimum dimensions of parallel-hole, multiaperture collimators for gamma-ray cameras. *J Nucl Med* 9: 233–235, 1968

6. KIBBY PM: The design of multichannel collimators for radioisotope cameras. *Brit J Radiol* 42: 91–101, 1969

7. JAHNS E, HINE GJ: A line-source phantom for testing the performance of scintillation cameras. *J Nucl Med* 8: 829–836, 1967

8. LORENZ WJ, SCHMIDLIN P, KAMPMANN H, et al: Comparative investigations with the Anger scintillation camera and the digital autofluoroscope. In *Medical Radioisotope Scintigraphy,* vol 1, Vienna, IAEA, 1969, pp 135–144

9. ANGER HO: Radioisotope Cameras. In *Instrumentation in Nuclear Medicine,* Hine GJ, ed, New York, Academic Press, 1967, pp 520–527

10. MUEHLLEHNER G: A diverging collimator for gamma-ray imaging cameras. *J Nucl Med* 10: 197–201, 1969

11. GREGG EC: Modulation transfer function, information capacity and performance criteria of scintiscans. *J Nucl Med* 9: 116–127, 1968

12. TREVES S, SPENCER R: Scanning phantom allowing planar and depth responses. *Invest Radiol* 5: 368, 1970

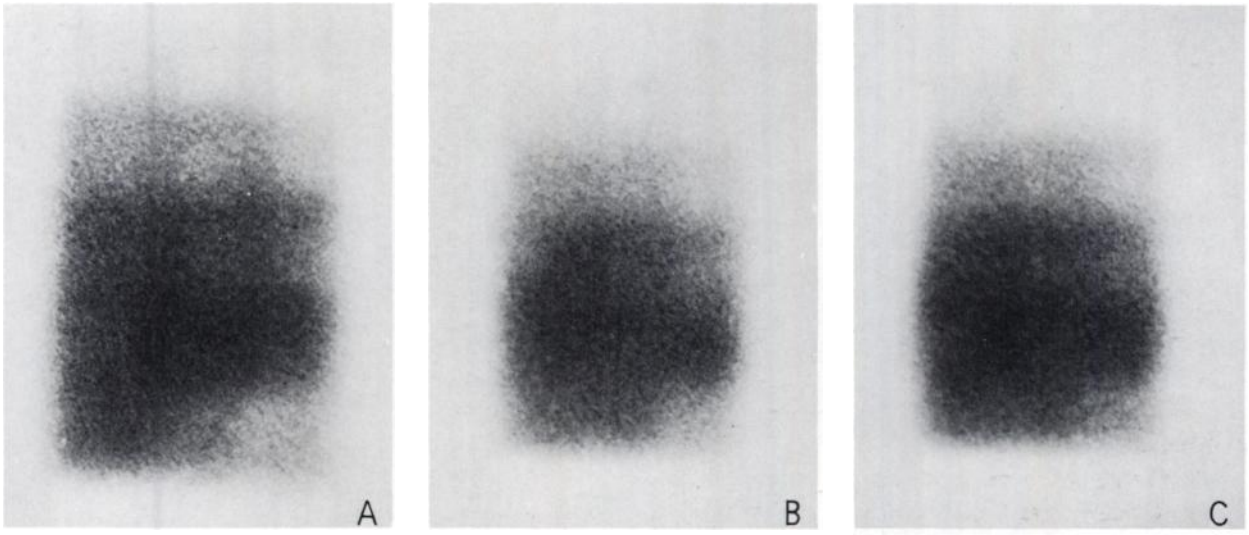

FIG. 5. A, B, and C show images of volume phantom with ^{99m}Tc using magnifying 1,000-hole (MB1K), straight-bore 1,000-hole (SB1K), straight-bore 4,000-hole (SB4K) collimators, respectively where same number of counts were collected for all pictures.